

## Article

# Application of Multiharmonic QCM-D for Detection of Plasmin at Hydrophobic Surfaces Modified by $\beta$ -Casein

Sandro Spagnolo <sup>1</sup>, Eric S. Muckley <sup>2</sup>, Iliia N. Ivanov <sup>2</sup> and Tibor Hianik <sup>1,\*</sup>

<sup>1</sup> Faculty of Mathematics, Physics and Informatics, Comenius University, Mlynska Dolina F1, 842 48 Bratislava, Slovakia; sandrospagnolo1@gmail.com

<sup>2</sup> Center for Nanophase Materials Sciences, Oak Ridge National Laboratory, P.O. Box 2008, Oak Ridge, TN 37831-6496, USA; ericmuckley@gmail.com (E.S.M.); ivanovin@ornl.gov (I.N.I.)

\* Correspondence: tibor.hianik@fmph.uniba.sk

**Abstract:** Plasmin protease plays an important role in many processes in living systems, including milk. Monitoring plasmin activity is important for control of the nutritional quality of milk and other dairy products. We designed a biosensor to detect the proteolytic activity of plasmin, using multiharmonic quartz crystal microbalance with dissipation (QCM-D). The  $\beta$ -casein immobilized on the hydrophobic surface of 1-dodecanethiol on the AT-cut quartz crystal was used to monitor plasmin activity. We demonstrated detection of plasmin in a concentration range of 0.1–20 nM, with the limit of detection about  $0.13 \pm 0.01$  nM. The analysis of viscoelastic properties of the  $\beta$ -casein layer showed rapid changes of shear elasticity modulus,  $\mu$ , and coefficient of viscosity,  $\eta$ , at plasmin sub-nanomolar concentrations, followed by modest changes at nanomolar concentrations, indicating multilayer architecture  $\beta$ -casein. A comparative analysis of viscoelastic properties of  $\beta$ -casein layers following plasmin and trypsin cleavage showed that the higher effect of trypsin was due to larger potential cleavage sites of  $\beta$ -casein.

**Keywords:** acoustic sensor; plasmin; trypsin;  $\beta$ -casein; cleavage; QCM-D; multiharmonic analysis; viscoelasticity



**Citation:** Spagnolo, S.; Muckley, E.S.; Ivanov, I.N.; Hianik, T. Application of Multiharmonic QCM-D for Detection of Plasmin at Hydrophobic Surfaces Modified by  $\beta$ -Casein. *Chemosensors* **2022**, *10*, 143. <https://doi.org/10.3390/chemosensors10040143>

Academic Editor: Barbara Palys

Received: 15 March 2022

Accepted: 9 April 2022

Published: 11 April 2022

**Publisher's Note:** MDPI stays neutral with regard to jurisdictional claims in published maps and institutional affiliations.



**Copyright:** © 2022 by the authors. Licensee MDPI, Basel, Switzerland. This article is an open access article distributed under the terms and conditions of the Creative Commons Attribution (CC BY) license (<https://creativecommons.org/licenses/by/4.0/>).

## 1. Introduction

Milk is a highly nutritional food composed of biologically active molecules that include proteases responsible for catalytic breakdown of the peptide bond of proteins, which in turn changes organoleptic properties of milk [1,2]. Consequently, the detection of the enzymatic activity of milk proteases is crucial for the control of nutritional properties of milk during its processing in the dairy industry [3,4]. Other non-enzymatic proteins in milk, such as caseins and whey proteins, are also important from a nutritional and technological point of view.

In an acid environment at pH 4.6, caseins tend to precipitate, while whey proteins remain in solution according to their primary structure and on the basis of post-translational modifications such as phosphorylation and glycosylation [5]. Caseins are the most abundant proteins in milk. They are organized in micellar macrostructures consisting of sub-micelles characterized by a hydrophilic surface and hydrophobic core. Caseins are divided into four groups based on their behavior in the presence of calcium ions:  $\alpha_{s1}$ - and  $\alpha_{s2}$ -caseins precipitate in the presence of low calcium concentrations (6 and 2 mM, respectively, at 1% protein concentration, pH 7),  $\beta$ -casein precipitates with medium calcium concentrations (approximately 15 mM), while  $\kappa$ -casein precipitates at higher calcium concentrations [6]. In this work  $\beta$ -casein was used as a substrate to study the proteolytic activity of plasmin. The monitoring of this protease is important, as the cleavage of  $\beta$ -casein causes alterations in the stability and coagulation properties of milk, which is important for the processing of dairy products. Plasmin is also responsible for nutritional changes in milk due to the formation of bioactive peptides following the proteolytic cleavage of caseins.

These peptides can provide particular nutraceutical characteristics, such as antimicrobial, antioxidant and immunomodulatory effects, but can also induce allergic reactions or intolerance in some predisposed individuals [4,7]. In addition, the high protease activity can cause the formation of precipitates or gelatinous portions in milk following heat treatment, which is not desirable for dairy production. The proteases present in milk can be of an endogenous nature (native in milk) or exogenous (produced by psychrotrophic bacteria) [8]. While it is possible to control the presence of exogenous proteases by acting on the viability of the bacteria, the presence of endogenous proteases is harder to control and is not always possible to monitor [9]. It is therefore important to design sensors capable of detecting the concentration and activity of the plasmin. This serine protease is in milk and blood mainly as an inactive zymogen (plasminogen), and both are heat stable, unlike their inhibitors and activators [10]. Plasmin can hydrolyze caseins, but it does not easily hydrolyze whey proteins. It also has a physiological role in lactation and in the digestion of milk [11]. Consequently, the development of the sensor for monitoring the plasmin activity is important for quality control of the dairy products.

Various approaches were reported for the detection of plasmin and its activity. This includes in particular fluorescence spectroscopy, which uses fluorogenic peptides as a substrate for plasmin cleavage [12]. For example, Dacres et al. designed a bioluminescence resonance energy transfer (BRET)-based biosensor for plasmin detection. Following proteolytic activity by the plasmin, the initial BRET ratio decreased with increasing plasmin concentration. This allowed a limit of detection (LOD) of 0.86 nM for bovine plasmin in whole milk to be determined [13]. Plasmin has also been detected by electrochemical sensors. For this purpose Ohtsuka et al. [14] used a specific peptide substrate modified at NH<sub>2</sub>-terminal by ferrocene (Fc) as a redox label and at C-terminal by cysteine. The cysteine residues allowed chemisorption of the peptides at the gold electrode. The cleavage of peptides by plasmin resulted in a decrease of the amplitude of the ferrocene redox current, which served as analytical signal. Using this method, they found a LOD of 50 ng/mL (0.57 nM). Castillo et al. used this approach for detection of plasmin in milk with LOD of  $0.56 \pm 0.03$  nM. This was much lower in comparison with optical UV-Vis detection method (LOD =  $3.68 \pm 0.04$  nM) [15]. For practical applications, and especially for the detection of the plasmin in non-transparent liquids such as milk, the acoustics methods are very useful. In this case the substrate for plasmin cleavage, such as short peptides or  $\beta$ -casein, are immobilized at the piezoelectric transducer. The cleavage of the substrate resulted in loss of mass and increase of the resonant frequency of acoustic sensor. Sensors of this type are based on acoustic waves such as thickness shear mode (TSM), quartz crystal microbalance (QCM) and electromagnetic piezoelectric acoustic sensor (EMPAS). All these methods were used for detection plasmin or trypsin (see Dizon et al. for recent review [16]). For example, using the EMPAS, Románszki et al., designed a sensor for plasmin based on a  $\beta$ -casein layers formed at hydrophobic surfaces of octadecanethiol. This approach substantially increased sensitivity of plasmin detection because the hydrophilic groups of  $\beta$ -casein were exposed to the water environment and therefore were more accessible to plasmin. The sensitivity of this method allowed detection of plasmin at concentration 32 pM [17]. Poturnayova et al. designed a QCM biosensor for plasmin using peptide substrate [18] or  $\beta$ -casein layers [19] immobilized at the thin gold layers of the piezocrystal. A LOD of 0.65 nM (peptide substrate) and 0.17 nM ( $\beta$ -casein) were reported. Similarly, Tatarko et al. used a  $\beta$ - and  $\kappa$ -casein layers to identify the differences in the activity of trypsin and plasmin. A machine learning algorithm allowed detection of plasmin within less than 2 min and a LOD of 0.5 nM [20].

In this work, a  $\beta$ -casein layer was adsorbed on the hydrophobic surface formed by 1-dodecanethiol chemisorbed at the thin gold layer of AT-cut quartz. In contrast with previous works, the QCM method with dissipation (QCM-D) at multiharmonic mode has been used. This approach allowed not only the detection of plasmin activity, but also the analysis of the changes of viscoelastic properties of  $\beta$ -casein layers during the cleavage by plasmin. Moreover, using the Voinova–Voigt viscoelastic model [21,22], it was

possible to quantify the variations of viscoelastic parameters during plasmin cleavage and to describe the architecture of the  $\beta$ -casein layer. The viscoelastic properties of  $\beta$ -casein layers following plasmin cleavage were compared with those caused by trypsin using the results of a recently published paper [23].

## 2. Materials and Methods

### 2.1. Chemicals

The aqueous solutions were prepared using deionized water produced by Pure Lab Classic UV (Elga Water Systems, High Wycombe, UK) and filtered with a 0.22  $\mu\text{m}$  membrane filter (Merck-Millipore, Darmstadt, Germany). Tris(hydroxymethyl)aminomethane (TRIS, Trizma<sup>®</sup> base, Sigma-Aldrich, Darmstadt, Germany) buffer 10 mM of pH 7.0 was used in all aqueous solutions with pH adjustment achieved by adding a few drops of concentrated HCl in deionized water. Bovine  $\beta$ -casein was purchased from Sigma-Aldrich ( $\geq 98\%$ ,  $M_w \approx 24,000$  g/mol) and solubilized in the TRIS buffer at a concentration of 0.1 mg/mL. Bovine plasmin (PLA) ( $M_w \approx 88,092$  g/mol) was obtained from Roche Diagnostics (Mannheim, Germany). The plasmin concentrations in the TRIS buffer used in the experiments were in the range 0.1–20 nM. 1-dodecanthiol (DDT) was purchased from Sigma-Aldrich ( $\geq 98\%$ ) and used for the preparation of a hydrophobic self-assembled monolayer (SAM) chemisorbed on QCM gold electrodes. Hydrogen peroxide (30%  $\text{H}_2\text{O}_2$ ), ammonia (26%  $\text{NH}_4\text{OH}$ ), 96% ethanol, HCl and NaOH powder were obtained from Slavus (Bratislava, Slovakia). All reagents and solvents were used without further purification.

### 2.2. Cleaning of QCM Crystals and Preparation of $\beta$ -Casein Layers

Prior to sensor preparation, the AT-cut QCM crystals with gold electrodes on both sides (Total Frequency Control Ltd., Storrington, UK, working area, 0.2  $\text{cm}^2$ , with fundamental resonance frequency of 8 MHz) were carefully cleaned with a Piranha basic solution (26%  $\text{NH}_4\text{OH}$ : 30%  $\text{H}_2\text{O}_2$ :  $\text{H}_2\text{O}$  in volume ratio 1:1:5) for 25 min followed by rinsing with deionized water. They were then rinsed with ethanol and dried under nitrogen flow. Then, the crystals were introduced into an incubation chamber to which a 0.5 mL of 1 mM of 1-dodecanethiol dissolved in ethanol had been added. The chambers were sealed with parafilm (Sigma-Aldrich) kept overnight at room temperature ( $20 \pm 2$  °C). The crystals were then rinsed with ethanol and dried under a nitrogen flow.

### 2.3. Experimental Set-Up

The crystal with immobilized DDT were mounted in an acrylic flow-through cell of a volume of approximately 100  $\mu\text{L}$  (JKU Linz, Austria). The gold electrodes of the piezoelectric disc were connected to a SARK-110 vector analyzer (Seeed, Shenzhen, China) by means of a coaxial cable. This device was connected to a computer via USB communication for control and data acquisition via software written in Python [24]. In this configuration, only one side of the crystal was exposed to the liquid. During the measurements, the crystals were held upright and in flow mode using a GeniePlus syringe pump (Kent Scientific, Torrington, CT, USA) to draw solutions directly from a vial. The liquids flowed into the cell chamber via an inlet tube and flowed away via an outlet tube towards the pulling syringe.

### 2.4. Measurements of the Resonant Frequency and Their Overtones

The vector analyzer allowed monitoring of all steps of the preparation of  $\beta$ -casein layers and their cleavage by plasmin. The measurements were performed at room temperature ( $20 \pm 2$  °C) at a flow rate of 50  $\mu\text{L}/\text{min}$ . Initially, ethanol and then TRIS buffer were flushed into the QCM flow cell to remove any excess of weakly adsorbed DDT molecules on the surface and to obtain a stable initial signal for a time corresponding to about 55–60 min. Meanwhile,  $\beta$ -casein and plasmin solutions were freshly prepared before their injection in the flow cell. The sample flow was stopped when the solutions had to be changed. After each solution change, a certain stabilization time was necessary before proceeding to the next step, except in the case of plasmin incubation, as it was decided that less time

was needed to visualize enzyme activity. After the initial TRIS buffer wash, the crystal was incubated with 0.1 mg/mL  $\beta$ -casein solution for 45 min until the signal reached its stabilization. A low concentration of  $\beta$ -casein was necessary to form a protein monolayer, because at higher concentrations the protein forms micelles and prevents the formation of a compact layer [17]. Then, the crystal was washed with TRIS buffer to remove the weakly bound  $\beta$ -casein until a stable frequency of the QCM was reached. Finally, 0.1–20 nM plasmin solutions were flowed over the surface bound  $\beta$ -casein. Each QCM crystal with  $\beta$ -casein layer was then incubated with one plasmin concentration for 30 min. Subsequently, the surface was rinsed with TRIS buffer to remove the plasmin and stop the enzymatic reaction until a stable baseline was obtained. Multifrequency analysis was carried out for all measurements, starting from the fundamental resonance frequency, 8 MHz and the following four overtones (3rd, 5th, 7th, 9th corresponding to 32 MHz, 35 MHz, 56 MHz and 72 MHz). The multiharmonic QCM-D method allows gravimetric measurements on the thin film simultaneously with the stiffness of the layer, thus allowing quantitative characterization of the protein adlayer before and after the plasmin enzymatic activity. Using traditional QCM, it is impossible to simultaneously calculate the viscoelastic values of  $\beta$ -casein layers.

### 2.5. The Basic Parameters of QCM and the Analysis of the Viscoelastic Properties of the Protein Layers

Since the experiments carried out made it possible to obtain information on the variations in resonance frequencies and dissipation, it is necessary to explain some physical properties related to these values. Among them, the important relationship that exists between the variation of the resonance frequency and the mass adsorbed on the surface of the crystal is described by the Sauerbrey equation [25].

$$\Delta f = -\frac{2nf_0^2}{\sqrt{\rho_q\mu_q}} \frac{\Delta m}{A} \quad (1)$$

where  $\Delta f$  (Hz) is the change of the resonance frequency,  $n$  and  $f_0$  are the overtone number and the fundamental frequency, respectively,  $\Delta m$  is the variation of the mass adsorbed on the surface,  $A$  is the active area of the quartz crystal,  $\mu_q$  and  $\rho_q$  are the shear modulus ( $2.947 \times 10^{10}$  Pa) and the density ( $2.648 \times 10^3$  kg m<sup>-3</sup>) of the quartz, respectively [25]. This equation is strongly valid for thin rigid layers in a vacuum. However, for crystal that made contact with liquid, the viscosity caused dissipation of the acoustic wave, which affected the resonance frequency. Therefore, analysis of the changes in the frequency and dissipation is also important for the study of the viscoelastic properties of the organic layers at the crystal surface contacted with aqueous solution. Most recently we applied multiharmonic analysis of viscoelastic properties of  $\beta$ -casein layers following cleavage by trypsin [23]. This analysis has been based on a Voinova–Voigt model using following equations [21,22]:

$$\Delta f \approx -\frac{1}{(2\pi\rho_0h_0)} \left[ \left( \frac{\eta_3}{\Gamma_3} \right) + h_1\rho_1\omega - 2h_1 \left( \frac{\eta_3}{\Gamma_3} \right)^2 \left( \frac{\eta_1\omega^2}{\mu_1^2} + \omega^2\eta_1^2 \right) \right] \quad (2)$$

$$D \approx \frac{1}{(\pi f_n\rho_0h_0)} \left[ \left( \frac{\eta_3}{\Gamma_3} \right) + 2h_1 \left( \frac{\eta_3}{\Gamma_3} \right)^2 \left( \frac{\eta_1\omega}{\mu_1^2} + \omega^2\eta_1^2 \right) \right] \quad (3)$$

where  $\omega$  is the angular frequency of the acoustic wave,  $\rho_0$  and  $h_0$  are the density and the thickness of the QCM crystal, respectively, and  $\eta_1$ ,  $\rho_1$ ,  $h_1$ , and  $\mu_1$  are the viscosity, density, thickness and shear elastic modulus of the adlayer. For proteins, an average density is  $1.35 \times 10^3$  kg m<sup>-3</sup> and the thickness of the protein layer can be obtained by dividing the mass per unit of area by density.  $\Gamma_3$  is the decay length of the shear wave in liquid expressed as:  $\Gamma_3 = \sqrt{\frac{2\eta_3}{\omega\rho_3}}$  [26].  $\rho_3 = 998.2$  kg/m<sup>3</sup> and  $\eta_3 = 1.0016$  mPa s are the density and dynamic viscosity of diluted aqueous solutions at 20 °C, respectively. The dissipation factor

is proportional to the decay length:  $D = \Gamma_3/f_0$  [27]. In the evaluation of the rigidity of the adlayer, the following criterium can be applied:

$$\frac{\Delta f_n}{n} \approx k \quad (4)$$

This relationship states that if the normalized frequency shift  $\Delta f_n/n$  is similar at different resonant frequencies, the adlayer fulfills stiffness criteria and the Sauerbrey equation can be used for mass calculations. Another criterion to verify that the adlayer is rigid or viscoelastic is based on the calculation of the ratio  $\Delta D_n/\Delta f_n$ . If this ratio is less than  $10^{-8} \text{ Hz}^{-1}$  [28], the adlayer can be considered rigid and it is possible to calculate its mass using Sauerbrey equation, while with a value greater than  $4 \times 10^{-7} \text{ Hz}^{-1}$  [29] the adlayer can be considered as viscoelastic. The adlayer can be considered rigid when the following relationship is true:

$$\frac{\Delta D_n}{\Delta f_n} \ll \frac{1}{f_0} \quad (5)$$

In this work the changes in frequency and dissipation of the QCM crystal were measured in multiharmonic mode to monitor the assembly of a  $\beta$ -casein layer and its cleavage by plasmin. It was demonstrated that the  $\beta$ -casein layer can be used for label-free detection of the plasmin proteolysis. Furthermore, by means of the Voinova–Voigt viscoelastic model [22,30], it was possible to quantify the changes in viscoelastic values and describe the architecture of the  $\beta$ -casein layer.

The measurements of the proteolytic activity at a given plasmin concentration were carried out at least three times. The reproducibility of the experiments was acceptable as it was demonstrated by a low standard deviation. Assembly of a single layer of  $\beta$ -casein led to similar frequency changes, suggesting similar packing density and acceptable reproducibility. The obtained data were fitted using a Python script that calculates the peak parameters using an equation from a work by Yoon et al. [31]. The fitted parameters were statistically processed and plotted using OriginPro 8 software (OriginLab Corporation, Northampton, MA, USA). All results are presented as mean  $\pm$  standard deviation (SD). The mass and thickness of the  $\beta$ -casein adlayer, before and after plasmin treatment, were calculated using the fitted data. The viscoelastic properties of the adlayer before and after enzyme incubation were also analyzed from fitting the data to the Voinova–Voigt viscoelastic model using Python code.

### 3. Results and Discussion

#### 3.1. The Formation of $\beta$ -Casein Layers and Their Cleavage by Plasmin

In the first series of experiments we studied the kinetics of the changes of resonant frequency and the overtones following formation of  $\beta$ -casein layers at the surface of 1-dodecanethiol (DDT) at the QCM transducer, as well following the addition of 10 nM plasmin. From Figure 1 it is seen that the kinetics of frequency changes can be divided into five phases that allow description of the sensor behavior after various surface modifications.

The first phase (1) corresponds to the stabilization of the frequency after washing the crystal surface covered by SAM from 1-dodecanethiol with TRIS buffer. The steady-state frequency has been then used as a baseline for the subsequent phenomena occurring at the surface. In the second phase (2), the crystal is incubated with a  $\beta$ -casein at a concentration of 0.1 mg/mL, below the critical micellar concentration ( $\text{CMC}_{\beta\text{-casein}} = 0.5 \text{ mg/mL}$  [32]). Thus, the protein layer has been formed from monomers of  $\beta$ -casein. It is seen that the resonant frequency decreases, evidencing  $\beta$ -casein adsorption on the hydrophobic DDT layer. Following the stabilization of the frequency, the crystal surface was rinsed again with the TRIS buffer. A slight increase in the resonances; frequency during the third phase (3) can be interpreted as a removal of weakly bound  $\beta$ -casein molecules from DDT surface [33]. Once the frequency stabilized, the  $\beta$ -casein layer was incubated with a plasmin at a concentration of 10 nM for 30 min (phase 4). Consequently,  $\beta$ -casein blank was omitted in Figure 2 because the incubation with the enzyme occurs when the signal has already

stabilized. The cleavage of  $\beta$ -casein by plasmin resulted in partial removal of the  $\beta$ -casein, which has been detected as an increase in the resonance frequency. In the last phase (5), rinsing of crystal surface was carried out with TRIS buffer until frequency stabilized. In order to compare changes in frequency for higher harmonics, we normalized frequency change, dividing it by overtone number  $n$ . The corresponding plot of the kinetics of the changes of normalized frequencies is presented on Figure 1b. It is seen here that the normalized curves do not overlap, evidencing viscosity contribution to frequency response. The changes in viscosity can be assessed by analyzing the changes in dissipation,  $\Delta D$ . The kinetics of the changes of dissipation at five frequencies are shown on Figure 2.

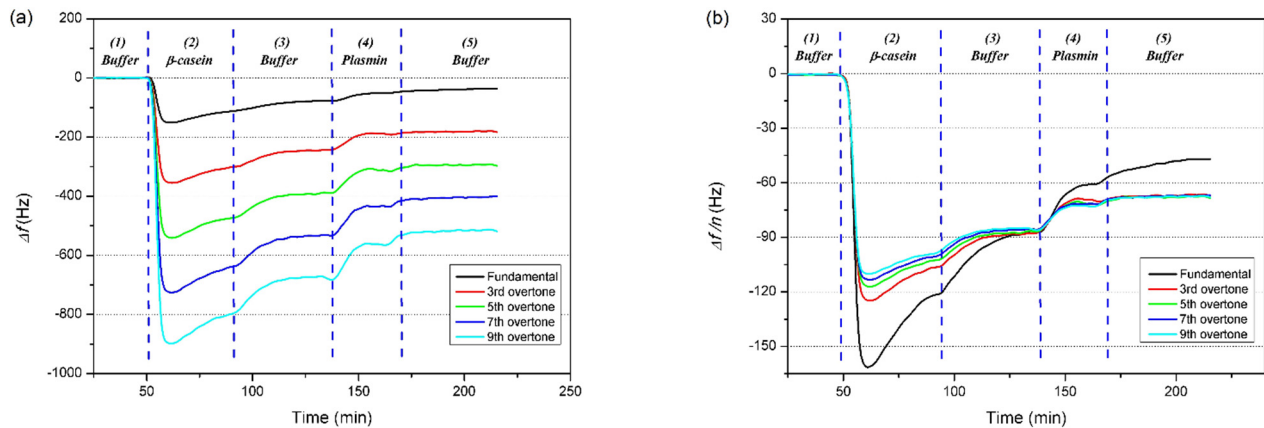


**Figure 1.** Plot of the kinetics of (a) resonant frequency and (b) overtone number-normalized frequency changes of the QCM crystal after incubation with different solutions: (1) rinsing of the 1-dodecanethiol-coated crystal with TRIS buffer; (2) incubation with 0.1 mg/mL of  $\beta$ -casein; (3) rinsing with TRIS buffer to remove weakly bound  $\beta$ -casein; (4) addition of plasmin in a concentration of 10 nM and incubation for 30 min; (5) rinsing with TRIS buffer.

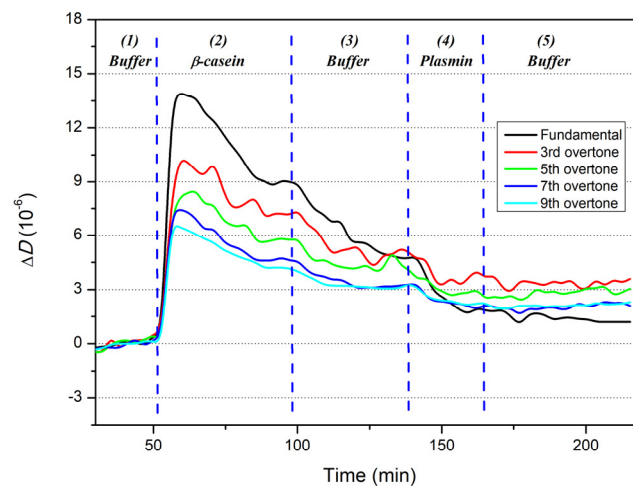


**Figure 2.** Plot of the dissipation changes,  $\Delta D$ , of the QCM crystal vs. time after incubation with different solutions at fundamental resonance frequency until 9th overtone: (1) initial rinsing of the 1-dodecanethiol-coated crystal with TRIS buffer; (2) incubation with 0.1 mg/mL  $\beta$ -casein; (3) rinsing with TRIS buffer to remove weakly bound  $\beta$ -casein; (4) incubation with plasmin at concentration of 10 nM for 30 min; (5) final rinsing with TRIS buffer.

The kinetics in the dissipation traces can also be divided into five phases. In contrast with the resonant frequency (Figure 1a), the dissipation increases after the first phase (1), followed by adsorption of  $\beta$ -casein on the second phase (2). This is due to the viscosity contribution of relatively soft  $\beta$ -casein layer. The observed overshoot at this phase may be due to the dynamic nature of  $\beta$ -casein assembly. At first it assembles as a soft layer (increases

in the dissipation), followed by ordering and rearrangement of the adlayer (decrease in the dissipation). After signal stabilization, the crystal was washed by TRIS buffer during the third phase (3), when reduction in dissipation was observed. We attribute this change in dissipation to the removal of weakly bound  $\beta$ -casein molecules. The incubation of the  $\beta$ -casein layer with a 10 nM plasmin for 30 min resulted in a decrease of the dissipation due to partial removal of the  $\beta$ -casein layer (phase 4). In the final phase (5), a rinsing of the surface of the crystal with a TRIS buffer was performed until a steady-state frequency was reached.

The average changes of  $D$  and  $f_n$  values of each stable baseline (phases 2, 3 and 5), with respect to the initial stabilization in phase (1), were determined for fundamental frequency and all overtones. The results are summarized in Table 1.

**Table 1.** Normalized resonance frequency changes from fundamental to the 9th overtone, after  $\beta$ -casein incubation (baseline 2 ( $b_2$ )), after rinsing (baseline 3 ( $b_3$ )) and after treatment with 10 nM plasmin concentration (baseline 5 ( $b_5$ )) compared to initial stabilization. The dissipation variation values obtained after the same baselines are also shown.

Parameter/ Harmonics No.	Fundamental	3rd	5th	7th	9th
$\Delta f_{b_2}/n$ , Hz	$-120.0 \pm 21.9$	$-113.8 \pm 3.8$	$-111.9 \pm 3.0$	$-104.0 \pm 3.1$	$-103.4 \pm 7.0$
$\Delta f_{b_3}/n$ , Hz	$-90.9 \pm 10.9$	$-89.3 \pm 3.7$	$-86.6 \pm 4.7$	$-83.8 \pm 4.5$	$-81.8 \pm 5.2$
$\Delta f_{b_5}/n$ , Hz	$-37.5 \pm 16.7$	$-61.5 \pm 2.4$	$-59.1 \pm 2.5$	$-58.6 \pm 3.7$	$-58.2 \pm 3.9$
$\Delta D_{b_2}$ , $10^{-6}$	$8.7 \pm 1.9$	$4.5 \pm 1.0$	$3.6 \pm 0.9$	$3.4 \pm 0.7$	$3.0 \pm 0.7$
$\Delta D_{b_3}$ , $10^{-6}$	$6.8 \pm 2.2$	$3.8 \pm 0.8$	$3.1 \pm 0.6$	$2.6 \pm 0.7$	$2.2 \pm 0.7$
$\Delta D_{b_5}$ , $10^{-6}$	$4.9 \pm 2.8$	$3.0 \pm 0.8$	$2.4 \pm 0.6$	$2.0 \pm 0.6$	$1.6 \pm 0.6$

### 3.2. Formation of $\beta$ -Casein Adlayer, Assessment of its Viscoelastic Nature and Applicability of the Sauerbrey Equation

The Sauerbrey Equation (1) allows calculation of the mass deposited on the QCM crystal and its portion removed due to the plasmin cleavage. The details of data analysis can be found in our recent publication focused on trypsin detection [23]. Here we will focus on the analysis of viscoelastic properties of the  $\beta$ -casein layers by plasmin cleavage.

Figure 1b shows that different harmonics do not overlap during the adsorption of the  $\beta$ -casein on the 1-dodecantethiol monolayer (phase 2). This suggests that the  $\beta$ -casein adlayer is not fully rigid and also exhibits viscous properties. However, after washing the surface by TRIS buffer, the harmonics overlap, suggesting that removal of the weakly bound  $\beta$ -casein diminishes the viscosity effect (phase 3). Following incubation of  $\beta$ -casein with plasmin, the adlayer undergoes mass loss (phase 5), and the harmonics tend to converge (overlap), except for the fundamental frequency, which does not show the same trend. This result agrees with our recently published data on the cleavage of  $\beta$ -casein by trypsin [23]. The overshoot at the beginning of the adlayer formation has already been observed and explained in other works [34,35].

The  $\Delta D_n/\Delta f_n$  ratio is a parameter commonly used for analysis of the adlayer rigidity [36]. The values of  $\Delta D_n/\Delta f_n$  obtained for higher harmonics (Table 2) satisfy the inequality (5) as they are less than  $1/f_0 = 1.25 \times 10^{-7} \text{ Hz}^{-1}$ . Consequently, the changes of the mass of  $\beta$ -casein adlayer was calculated and compared to previous studies.

**Table 2.** The relationships between the dissipation and frequency changes in the stabilizations of phases 2 ( $b_2$ ), 3 ( $b_3$ ) and 5 ( $b_5$ ) for fundamental frequency and for 3rd to 9th overtones.

Parameter/ Harmonics No.	Fundamental	3rd	5th	7th	9th
$\Delta D_{b_2}/\Delta f_{b_2}$ , $\text{Hz}^{-1}$	$7.2 \times 10^{-8}$	$4.0 \times 10^{-8}$	$3.2 \times 10^{-8}$	$3.3 \times 10^{-8}$	$2.9 \times 10^{-8}$
$\Delta D_{b_3}/\Delta f_{b_3}$ , $\text{Hz}^{-1}$	$7.5 \times 10^{-8}$	$4.2 \times 10^{-8}$	$3.6 \times 10^{-8}$	$3.2 \times 10^{-8}$	$2.7 \times 10^{-8}$
$\Delta D_{b_5}/\Delta f_{b_5}$ , $\text{Hz}^{-1}$	$1.3 \times 10^{-7}$	$4.9 \times 10^{-8}$	$4.1 \times 10^{-8}$	$3.3 \times 10^{-8}$	$2.8 \times 10^{-8}$

The changes in 3rd, 5th and 7th overtones (phase 2, Figure 1) have been used for estimation of the mass changes using Equation (1). However, the 9th harmonic was not used in the calculation since, as it can be seen in Figure 1b, this overtone tends to overlap with the previous harmonics at baselines in all the measurements performed. Therefore, in order to avoid data redundancy and repetition of calculations with the same values; only overtones until the 7th were considered.

The average frequency changes corresponded to the formation of  $\beta$ -casein layer (Figure 1b, phases 2–3) were determined as  $\Delta f_n = 86.6 \pm 5.2$  Hz. According to the Sauerbrey Equation (1), this corresponds to the mass density of the  $\beta$ -casein adlayer  $6.0 \pm 0.4$  mg/m<sup>2</sup>. The obtained value correlates well with those reported in the literature [17,23,35,37]. The adsorbed mass density before the buffer rinse was  $7.5 \pm 0.4$  mg/m<sup>2</sup>, corresponding to the structure of a double layer in which the inner layer is denser than outer layer which is, however, partially removed after washing [33].

The thickness of the adsorbed layer,  $h_f$ , was quantified using the mass changes ( $\Delta m$ ), the active area of the QCM crystal ( $A = 0.2$  cm<sup>2</sup>) and the averaged density of a protein ( $\rho_p = 1.35$  g/cm<sup>3</sup>). The following equation was used for calculation of the layer thickness:

$$h_f = \frac{\Delta m}{A \cdot \rho_p} \quad (6)$$

The thickness of the adlayer after rinsing with the buffer was found to be  $4.4 \pm 0.3$  nm, compared to  $5.6 \pm 0.3$  nm before the wash [17,23,33,38,39].

The viscoelastic values of the  $\beta$ -casein adlayer were also calculated using the Voinova–Voigt model. The 1-dodecanetriol monolayer is thinner (1.6 nm) than the  $\beta$ -casein layer and smaller than the penetration depth (112 nm). This suggests that it does not significantly contribute to the viscoelastic values. In the case of bare QCM crystals immersed in water, the penetration depth ( $\Gamma_3$ ) is about 250 nm [40]. The value of penetration depth of 3rd overtone  $\Gamma_3$  for  $\beta$ -casein adlayer after TRIS washing has been calculated to be  $\Gamma_3 = 112.0 \pm 0.6$  nm, which is similar to the value of  $104 \pm 1$  nm obtained in our recent work [23].

The changes in viscosity coefficient ( $\eta$ ) and shear modulus ( $\mu$ ) of  $\beta$ -casein layer were also calculated. The following values were obtained:  $\mu = (6.4 \pm 1.3) \times 10^4$  Pa,  $\eta = (10.8 \pm 4.4) \times 10^{-4}$  Pa s. These values are of the same order of magnitude as those reported in the literature [41,42] as well as in our recent paper [23]. Considering that the results obtained are consistent with those published earlier, we continued the study of the effect of plasmin on the physical properties of the  $\beta$ -casein layer.

### 3.3. Effect of Plasmin on the Viscoelastic Properties of $\beta$ -Casein Adlayer

The results of the study of the kinetics of the changes in frequency,  $\Delta f_{Pla}$ , and dissipation,  $\Delta D$ , at various concentrations of plasmin (0.1–20 nM) are presented in Figure 3. As can be seen, with increased plasmin concentration the frequency increases (Figure 3a) and dissipation decreases (Figure 3b).

This clearly evidences the cleavage of the  $\beta$ -casein by the plasmin that causes a decrease of the mass of the casein adlayer and consequently increases the resonant frequency. The decrease of the dissipation is likely due to the removal of the outer, softer part of the  $\beta$ -casein layer.

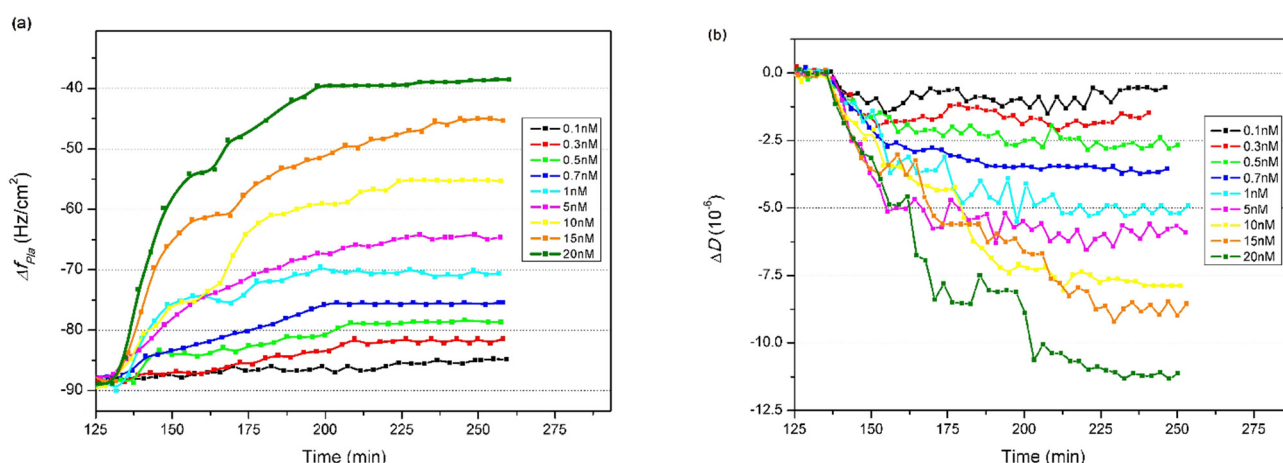


**Figure 3.** The kinetics of the changes of the 3rd harmonic frequency (a) and dissipation (b) at different concentrations of plasmin (see the legend) after the stabilization of the newly formed  $\beta$ -casein adlayer.

An inverse Michaelis–Menten model was used to analyze the variations of the 3rd overtone due to enzymatic activity. The fundamental frequency, as it had a wide variability due to greater sensitivity to spurious events occurring on the electrode borders, was not used in the analysis. Moreover, the harmonics higher than the 3rd were not included in the analysis because they tended to overlap. In this model, normalized ( $\Delta f_N$ ) frequency changes were used to minimize the variations in the amount of adsorbed  $\beta$ -casein,  $\Delta f_{casein}$ , according to the equation:

$$\Delta f_N = \frac{\Delta f_{Pla}}{\Delta f_{casein}} \cdot 100 (\%) \quad (7)$$

where  $\Delta f_{Pla}$  is the frequency change following the removal of  $\beta$ -casein from the QCM crystal surface by plasmin. Subsequently,  $\Delta f_N$  can be expressed as inverse Michaelis–Menten model [17]:

$$\Delta f_N = (\Delta f_N)_{MAX} \frac{[Pla]}{K_M + [Pla]} \quad (8)$$

where  $[Pla]$  is the plasmin concentration,  $(\Delta f_N)_{MAX}$  is the maximum frequency change in saturating conditions and  $K_M$  is the inverse Michaelis–Menten constant describing the plasmin concentration at which half of the maximum enzyme reaction speed is achieved. Using this equation, we fitted the experimental data presented in Figure 4a as a plot of  $\Delta f_N$  vs. concentration of plasmin. The Equation (8) can be linearized by the Lineweaver–Burk coordinates (Figure 4b), which allow the values of  $(\Delta f_N)_{MAX}$  and  $K_M$  to be independently determined from the linear fit. The following values were obtained from the linear fit (Figure 4b):  $(\Delta f_N)_{MAX} = 34.28 \pm 0.79\%$  and  $K_M = 0.90 \pm 0.02$  nM.

The limit of plasmin detection was calculated using the following relationship:  $LOD = 3.3 SD/\kappa$ , where  $(\kappa)$  is the slope of the curve of the graph in Figure 4a in the linear sub-nanomolar interval of plasmin and  $SD$  is the standard deviation of the y-intercept of the regression line for same concentration interval. We found these values to be  $\kappa = 12.11$  and  $SD = 0.13$  and the corresponding value of  $LOD$  was found to be  $0.13 \pm 0.01$  nM. The sensitivity of the developed biosensor is also sufficient for practical application considering that the plasmin concentration in cow's milk is approximately 5 nM [19]. The comparison of the sensitivity of plasmin detection by various methods is presented in Table 3.

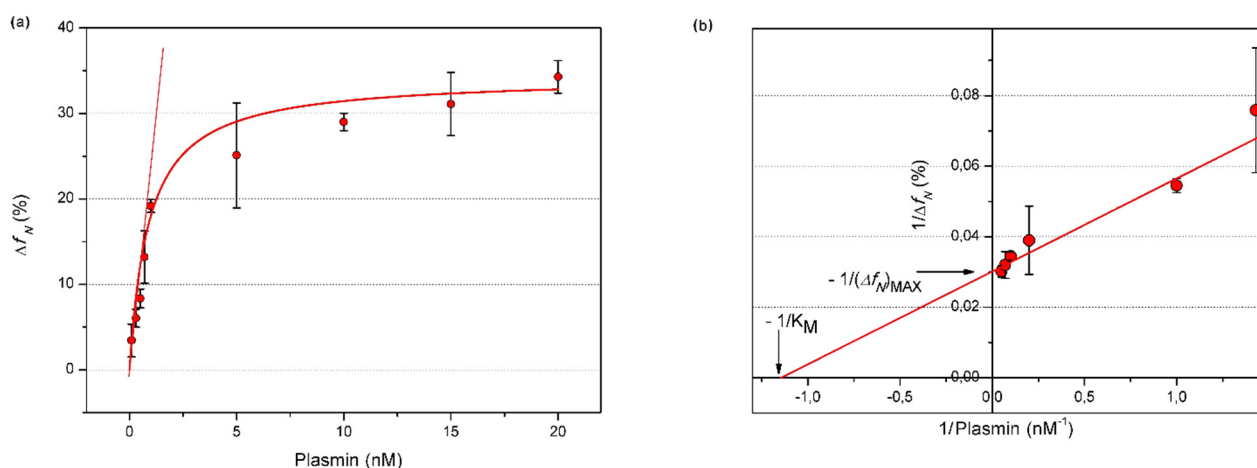


**Figure 4.** (a) The plot of the normalized frequency changes at different plasmin concentrations, fitted with inverse Michaelis–Menten equation. (b) Lineweaver–Burk plot obtained from the data of Figure 4a and linear fit using Origin Pro 8. The red lines are the fitted curves.

**Table 3.** Comparison of the results of studies conducted on the plasmin detection using different methods.

Substrate	Method of Detection	Plasmin Source	Assay Medium	Linear Range, nM	LOD, nM	Detection Time, min	$K_M$ , nM	Ref.
RLuc2-Peptide-GFP	BRET	Human	TB	0.09–3.29	0.03	10	ND	[13]
RLuc2-Peptide-GFP	BRET	Bovine	TB	0.48–8.41	0.26	10	ND	[13]
RLuc2-Peptide-GFP	BRET	Human	50% milk/TB	0.78–44.16	0.25	10	ND	[13]
RLuc2-Peptide-GFP	BRET	Bovine	50% milk/TB	1.19–29.92	0.86	10	ND	[13]
Chromogenic substrate *	Colorimetry	Human	50% milk/TB	ND	1.8	40	ND	[13]
Chromogenic substrate *	Colorimetry	Bovine	50% milk/TB	ND	0.5	40	ND	[13]
Short peptide	DPV	Human	0.2 M HClO <sub>4</sub>	1–12	0.6	60	ND	[14]
Short peptide	CV	Bovine	PB	1–2.5	0.56	60	2.5	[15]
Short peptide	CV	Bovine	Milk (2.8% fat)	1–2.5	0.6	60	0.8	[15]
Spectrozyme PL	Colorimetry	Bovine	PB	5–30	3.68	40	ND	[15]
$\beta$ -casein adlayer	EMPAS	Bovine	PB	0.032–10	0.032	30	3.29	[17]
Short peptide	QCM	Bovine	PB	1–20	0.65	30	ND	[18]
$\beta$ -casein	QCM	Bovine	PB	0.1–5	0.17	50	ND	[19]
$\beta$ -casein	QCM	Bovine	PB	1–10	0.5	>100	ND	[20]
$\kappa$ -casein	QCM	Bovine	PB	1–10	0.2	>100	ND	[20]
Fibrinogen-AuNPs	Colorimetry	Human	Human serum	0–50	0.4	60	ND	[43]
Fibrinogen-Au NPs on MCEM	LDI-MS	Human	PB	0–10	0.1	60	ND	[44]
Short peptide	Magnetic	Bovine	PB	0.001–11	0.12	2	ND	[45]
RLuc8.6-Peptide-TurboFP635	Optical, BRET	Human	Human plasma 7.5%	22.5–215.4	11.9	10	ND	[46]
$\beta$ -casein	Mechanical	Bovine	Water	0.33–13.3	0.7	>60	ND	[47]
$\beta$ -casein	Ultrasound spectroscopy	Bovine	PB	0.2–5	0.2	15–30	1.06	[48]
$\beta$ -casein	QCM	Bovine	PB	0.1–1.0	0.13	15–30	0.9	This work

BRET—bioluminescence resonance energy transfer; Chromogenic substrate \*—D-Val-Leu-Lys-4-nitroanilide dihydrochloride; CV—cyclic voltammetry; DPV—differential pulse voltammetry; Fib-AuNPs—fibrinogen-modified gold nanoparticles; GFP—green fluorescent protein;  $K_M$ —Michaelis–Menten constant; LDI-MS—pulsed-laser desorption/ionization mass spectrometry; MCEM—mixed cellulose ester membrane; RLuc2—Renilla luciferase; TB—TRIS buffer; PB—Phosphate buffer.

The sensitivity of acoustics methods of detection, Table 3, is close to the BRET techniques. An additional advantage of acoustic techniques is that they are label-free and can be used in non-transparent liquids such as raw milk.

We also analyzed the changes of the  $\beta$ -casein adlayer thickness,  $\Gamma_3$ , the viscosity coefficient,  $\eta$ , and the shear modulus,  $\mu$ , before and after the incubation of the  $\beta$ -casein layer with plasmin. The plot of these values as a function of plasmin concentration is

presented in Figure 5. As can be seen, the  $\beta$ -casein thickness, shear modulus (Figure 5a) and viscosity coefficient (Figure 5b) decrease with increasing plasmin concentration due to the partial removal of the  $\beta$ -casein adlayer. Furthermore, at low concentrations of plasmin, the viscoelastic coefficients decrease more rapidly. It is likely that, at the initial stage of incubation, the plasmin is able to remove the outer portion of the looser adlayer (more responsible for viscoelasticity), but probably does not cleave deeper due to the dilution of the enzyme. At higher plasmin concentrations, however, during the incubation time, the protease also begins to remove the inner layer of  $\beta$ -casein, but as it becomes denser, the viscoelastic values decrease less rapidly.

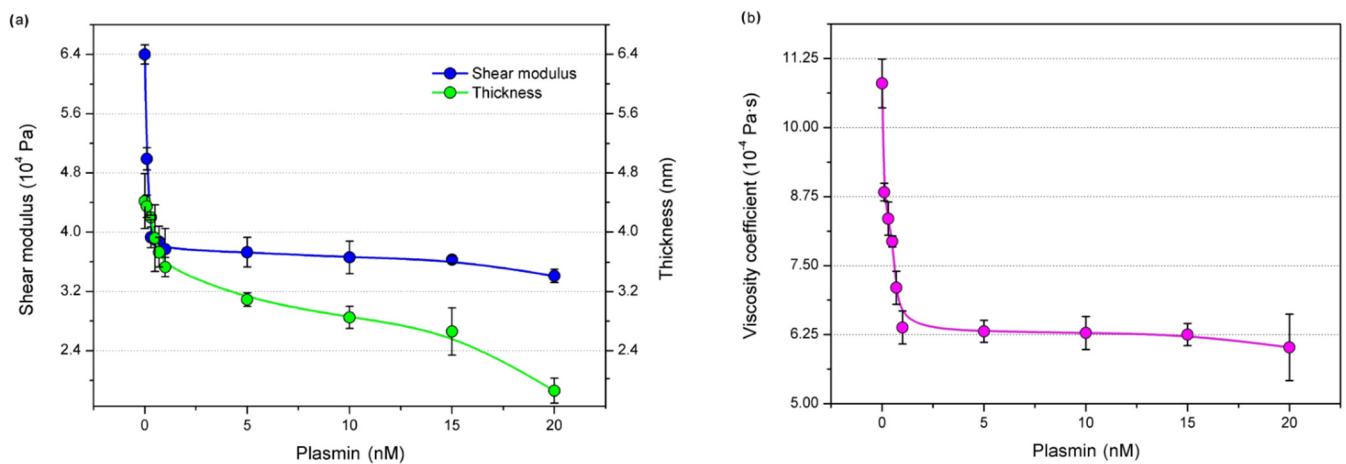


**Figure 5.** Variation of (a) thickness and shear modulus and (b) viscosity coefficient vs. concentration of the plasmin.

It is interesting to compare the effect of plasmin on the viscoelastic properties of  $\beta$ -casein layers with those by trypsin reported in our recent paper [23]. The plot of the effect of plasmin and trypsin on the changes of shear modulus and viscosity coefficient as a function of protease concentration is presented on Figure 6. It can be seen that the changes of both viscoelastic values are similarly rapid at a picomolar range of the protease concentration. However, at higher, nanomolar concentrations the effect of trypsin on shear modulus is higher (Figure 6a), but the coefficient of elasticity is lower than those caused by plasmin (Figure 6b). The rapid changes in the viscoelastic values at picomolar concentration range can be attributed to the cleavage of N-terminal regions of casein presumably to the outer layer, which is most exposed in the bulk solution.

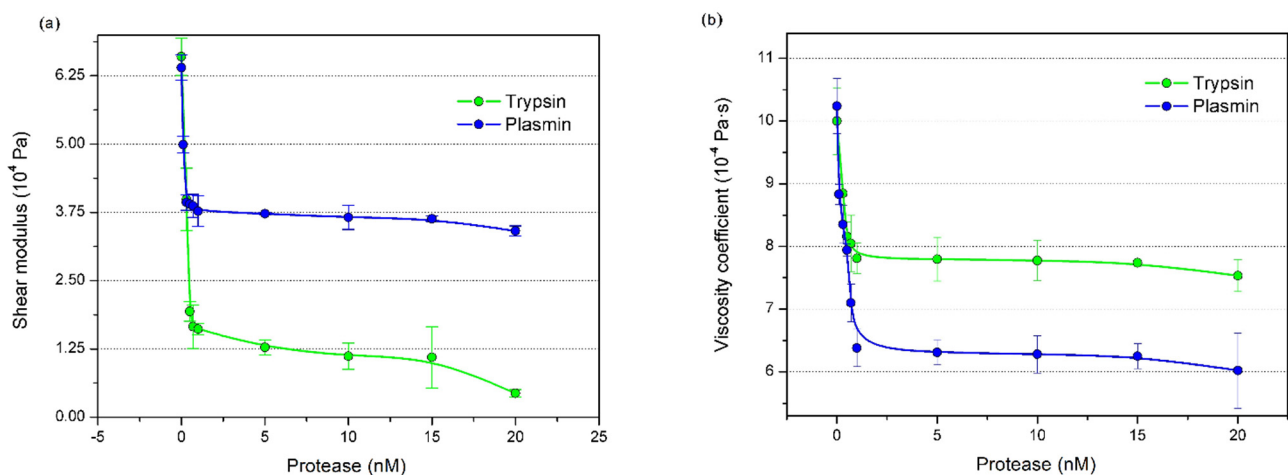


**Figure 6.** The plot of (a) shear modulus and (b) viscosity coefficient vs. concentration of trypsin and plasmin analyzed by Voinova–Voigt model.

The differences in behavior of viscoelastic values at nanomolar concentrations of proteases can be interpreted considering the nature of their interaction with  $\beta$ -casein. Trypsin cleaves proteins from the C side of a lysine or arginine, while plasmin preferentially cleaves the lysine bond. As a result, trypsin appears to cleavage  $\beta$ -casein more than plasmin, with 15 potential cleavage sites versus 11 in the case of plasmin [49]. However, the most interesting finding is that the trypsin exclusive cleavage sites are preferentially found in the highly hydrophobic carboxyl terminal region of casein. This is schematically showed in Figure 7. Thus, the portion of potential cleavage sites of  $\beta$ -casein for trypsin is localized more internally in the  $\beta$ -casein adlayer and is therefore less easily reached by trypsin (shown by the red arrows in Figure 7).

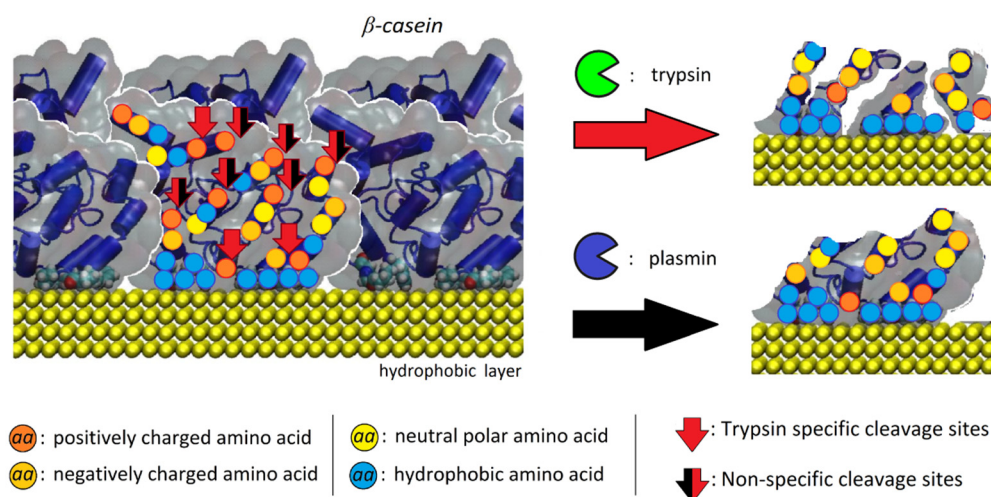


**Figure 7.** The scheme of cleavage sites for trypsin and plasmin at  $\beta$ -casein formed at hydrophobic surface and the scheme of  $\beta$ -casein layer after cleavage by proteases.

Accordingly, at nanomolar trypsin concentrations the proteolytic activity of the hydrophobic region of  $\beta$ -casein (C-terminal) increases, and the resulting hydrophobic fragments tend to remain attached to the electrode surface [50].

This would explain the differences in the adlayer viscoelasticity coefficients in the two experiments: a more hydrophobic fragmented  $\beta$ -casein layer could have a lower shear modulus than a more intact layer, as the elasticity of the material is also due to the nature and number of chemical bonds. In addition, such a layer could disperse more acoustic energy (since it would become less compact) and therefore result in the increase of the viscosity coefficient, in comparison with the layer exposed to plasmin. Since these two enzymes differently interact with the  $\beta$ -casein layer, there is the possibility for the designed biosensors to discriminate contributions from trypsin and plasmin in the presence of both proteases in a sample. The data analytics could be conducted through advanced statistics or machine learning algorithm using unique signatures of interaction [20]. We should mention that the main focus of this study was on the analysis of viscoelastic properties of the  $\beta$ -casein following cleavage by plasmin and trypsin. High sensitivity of QCM-D method and simplicity of implementation supports practical applications of this approach for the detection of plasmin in real milk samples. The QCM method has been already demonstrated for plasmin detection in milk, which is similar to the detection in the buffer [19]. The problem of plasmin detection in real milk samples is because plasmin is associated with casein micelles, requiring an additional step for the plasmin isolation for the following detection.

#### 4. Conclusions

The multiharmonic QCM-D method enabled detection of plasmin with LOD of  $0.13 \pm 0.01$  nM and an estimation of an inverse Michaelis–Menten constant,  $K_M = 0.90 \pm 0.02$  nM.

Using changes in the 3rd overtone of QCM, the variation in thickness, shear modulus and viscosity coefficient of  $\beta$ -casein adlayer following cleavage by plasmin was analyzed. We showed that  $\beta$ -casein assembles on the hydrophobic surfaces as an asymmetrical double layer in which the innermost layer is denser than the outermost one. The comparative analysis indicates that  $\beta$ -casein can adapt different conformations through the thickness of the layer, so that the innermost zone is made up of the most hydrophobic regions and the outermost layer is hydrophilic. Further research will target experiments to verify this concept.

The detailed analysis of the dynamics of the  $\beta$ -casein cleavage by plasmin showed rapid changes of viscoelastic values and thickness at relatively low (<2 nM) plasmin concentrations, which was attributed to the removal of the outer part of the looser  $\beta$ -casein layer, which does disturb the denser inner  $\beta$ -casein layer. The latter is removed at higher plasmin concentration.

The comparative analysis of the effect of trypsin and plasmin on the viscoelastic properties of the  $\beta$ -casein layer confirms the casein layered architecture. Exposure of the protein layer to these enzymes resulted in a different trend in the variation of the shear modulus and the viscosity coefficient of the adlayer due to different cleavage sites of these proteases. Trypsin has four more potential cleavage sites on  $\beta$ -casein than the plasmin with two sites located in the hydrophobic C-terminal region of the protein. Enzyme access to these sites does not lead to the removal of  $\beta$ -casein but affects its viscoelastic properties.

In summary, the multiharmonic analysis of QCM-D data demonstrated: (1) the detection of plasmin in subnanomolar concentration range, comparable with the most sensitive EMPAS and fluorescence detection methods; (2) the possibility of following the dynamic changes of viscoelastic properties and the thickness of  $\beta$ -casein layer during the cleavage by plasmin. Thus, the multiharmonic QCM-D methods could be beneficial for studying the mechanisms of the protease activity at surfaces at various conditions.

Lastly, vibrational methods such as infrared spectroscopy or Raman spectroscopy can also be used for the study of the enzymatic activity of proteases on  $\beta$ -casein and these tasks are the subject of further work. However, the cost-effectiveness and simplicity of the analysis conducted in this work makes the QCM-D method and the use of a  $\beta$ -casein layer a good candidate for plasmin monitoring.

**Author Contributions:** Conceptualization, S.S., I.N.I. and T.H.; formal analysis, S.S. and E.S.M.; investigation, S.S.; methodology, S.S., E.S.M., I.N.I. and T.H.; validation, S.S.; funding acquisition, I.N.I. and T.H.; project administration, I.N.I. and T.H.; software, E.S.M.; supervision, I.N.I. and T.H.; writing—original draft, S.S.; writing—review & editing, S.S., E.S.M., I.N.I. and T.H. All authors have read and agreed to the published version of the manuscript.

**Funding:** A portion of this research was conducted at the Center for Nanophase Materials Sciences, which is a DOE Office of Science User Facility, project No. CNMS2018-293. This work was funded under the European Union's Horizon 2020 research and innovation program through the Marie Skłodowska-Curie grant agreement No 690898 and by Science Agency VEGA, project No. 1/0419/20.

**Institutional Review Board Statement:** Not applicable.

**Informed Consent Statement:** Not applicable.

**Data Availability Statement:** Not applicable.

**Conflicts of Interest:** The authors declare no conflict of interest.

## References

1. Ianni, A.; Martino, G. Dietary grape pomace supplementation in dairy cows: Effect on nutritional quality of milk and its derived dairy products. *Foods* **2020**, *9*, 168. [[CrossRef](#)] [[PubMed](#)]
2. Datta, N.; Deeth, H.C. Diagnosing the cause of proteolysis in UHT milk. *LWT-Food Sci. Technol.* **2003**, *36*, 173–182. [[CrossRef](#)]
3. Yadav, J.S.S.; Yan, S.; Pilli, S.; Kumar, L.; Tyagi, R.D.; Surampalli, R.Y. Cheese whey: A potential resource to transform into bioprotein, functional/nutritional proteins and bioactive peptides. *Biotechnol. Adv.* **2015**, *33*, 756–774. [[CrossRef](#)] [[PubMed](#)]
4. Korhonen, H.; Pihlanto, A. Bioactive peptides: Production and functionality. *Int. Dairy J.* **2006**, *16*, 945–960. [[CrossRef](#)]

5. Michalski, M.-C.; Januel, C. Does homogenization affect the human health properties of cow's milk? *Trends Food Sci. Technol.* **2006**, *17*, 423–437. [[CrossRef](#)]
6. Tessier, H.; Rose, D.; Marier, J. Turbidimetric method for estimating sum of  $\beta$ - and  $\kappa$ -caseins in whole casein. *J. Dairy Sci.* **1963**, *46*, 651–655. [[CrossRef](#)]
7. Albenzio, M.; Santillo, A.; Caroprese, M.; Della Malva, A.; Marino, R. Bioactive peptides in animal food products. *Foods* **2017**, *6*, 35. [[CrossRef](#)]
8. Sodhi, M.; Sharma, M.; Sharma, A.; Verma, P.; Mohanty, A.; Kataria, R.S.; Shandilya, U.K.; Kumari, P.; Mukesh, M. Expression profile of different classes of proteases in milk derived somatic cells across different lactation stages of indigenous cows (*Bos indicus*) and riverine buffaloes (*Bubalus bubalis*). *Anim. Biotechnol.* **2021**, 1–10. [[CrossRef](#)]
9. Fox, P. Exogenous enzymes in dairy technology—A review 1. *J. Food Biochem.* **1993**, *17*, 173–199. [[CrossRef](#)]
10. Denis, T.S.; Humbert, G.; Gaillard, J.-L. Heat inactivation of native plasmin, plasminogen and plasminogen activators in bovine milk: A revisited study. *Lait* **2001**, *81*, 715–729. [[CrossRef](#)]
11. Dalsgaard, T.; Heegaard, C.; Larsen, L. Plasmin digestion of photooxidized milk proteins. *J. Dairy Sci.* **2008**, *91*, 2175–2183. [[CrossRef](#)]
12. Pierzchala, P.A.; Dorn, C.P.; Zimmerman, M. A new fluorogenic substrate for plasmin. *Biochem. J.* **1979**, *183*, 555–559. [[CrossRef](#)]
13. Dacres, H.; Wang, J.; Anderson, A.; Trowell, S.C. A rapid and sensitive biosensor for measuring plasmin activity in milk. *Sens. Actuators B* **2019**, *301*, 127141. [[CrossRef](#)]
14. Ohtsuka, K.; Maekawa, I.; Waki, M.; Takenaka, S. Electrochemical assay of plasmin activity and its kinetic analysis. *Anal. Biochem.* **2009**, *385*, 293–299. [[CrossRef](#)]
15. Castillo, G.; Pribransky, K.; Mező, G.; Kocsis, L.; Csámpai, A.; Németh, K.; Keresztes, Z.; Hianik, T. Electrochemical and photometric detection of plasmin by specific peptide substrate. *Electroanalysis* **2015**, *27*, 789–798. [[CrossRef](#)]
16. Dizon, M.; Tatarko, M.; Hianik, T. Advances in analysis of milk proteases activity at surfaces and in a volume by acoustic methods. *Sensors* **2020**, *20*, 5594. [[CrossRef](#)]
17. Románszki, L.; Tatarko, M.; Jiao, M.; Keresztes, Z.; Hianik, T.; Thompson, M. Casein probe-based fast plasmin determination in the picomolar range by an ultra-high frequency acoustic wave biosensor. *Sens. Actuators B* **2018**, *275*, 206–214. [[CrossRef](#)]
18. Poturnayova, A.; Karpisova, I.; Castillo, G.; Mező, G.; Kocsis, L.; Csámpai, A.; Keresztes, Z.; Hianik, T. Detection of plasmin based on specific peptide substrate using acoustic transducer. *Sens. Actuators B* **2016**, *223*, 591–598. [[CrossRef](#)]
19. Poturnayova, A.; Szabo, K.; Tatarko, M.; Hucker, A.; Kocsis, R.; Hianik, T. Determination of plasmin in milk using QCM and ELISA methods. *Food Control* **2021**, *123*, 107774. [[CrossRef](#)]
20. Tatarko, M.; Muckley, E.S.; Subjakova, V.; Goswami, M.; Sumpter, B.G.; Hianik, T.; Ivanov, I.N. Machine learning enabled acoustic detection of sub-nanomolar concentration of trypsin and plasmin in solution. *Sens. Actuators B* **2018**, *272*, 282–288. [[CrossRef](#)]
21. Voinova, M.V.; Rodahl, M.; Jonson, M.; Kasemo, B. Viscoelastic acoustic response of layered polymer films at fluid-solid interfaces: Continuum mechanics approach. *Phys. Scr.* **1999**, *59*, 391. [[CrossRef](#)]
22. Voinova, M.V. The theory of acoustic sensors application in air quality control. *Urban Clim.* **2018**, *24*, 264–275. [[CrossRef](#)]
23. Spagnolo, S.; Muckley, E.S.; Ivanov, I.N.; Hianik, T. Analysis of trypsin activity at  $\beta$ -casein layers formed on hydrophobic surfaces using a multiharmonic acoustic method. *Analyst* **2022**, *147*, 461. [[CrossRef](#)] [[PubMed](#)]
24. Muckley, E.S.; Collins, L.; Srijanto, B.R.; Ivanov, I.N. Machine learning-enabled correlation and modeling of multimodal response of thin film to environment on macro and nanoscale using “lab-on-a-crystal”. *Adv. Funct. Mat.* **2020**, *30*, 1908010. [[CrossRef](#)]
25. Sauerbrey, G. Verwendung von schwingquarzen zur wägung dünner schichten und zur mikrowägung. *Z. Phys.* **1959**, *155*, 206–222. [[CrossRef](#)]
26. Ellis, J.S.; Thompson, M. Acoustic coupling at multiple interfaces and the liquid phase response of the thickness shear-mode acoustic wave sensor. *Chem. Commun.* **2004**, 1310–1311. [[CrossRef](#)]
27. Ballantine, D.S.; White, R.M.; Martin, S.J.; Ricco, A.J.; Zellers, E.T.; Frye, G.C.; Wohltjen, H. *Acoustic Wave Sensors: Theory, Design and Physico-Chemical Applications*, 1st ed.; Academic Press: San Diego, CA, USA, 1997; pp. 36–70.
28. Cho, N.-J.; Frank, C.W.; Kasemo, B.; Höök, F. Quartz crystal microbalance with dissipation monitoring of supported lipid bilayers on various substrates. *Nat. Protoc.* **2010**, *5*, 1096–1106. [[CrossRef](#)]
29. Reviakine, I.; Johannsmann, D.; Richter, R.P. Hearing what you cannot see and visualizing what you hear: Interpreting quartz crystal microbalance data from solvated interfaces. *Anal. Chem.* **2011**, *83*, 8838–8848. [[CrossRef](#)]
30. Vikström, A.; Voinova, M. Soft-film dynamics of SH-SAW sensors in viscous and viscoelastic fluids. *Sens. Biosens. Res.* **2016**, *11*, 78–85. [[CrossRef](#)]
31. Yoon, S.M.; Cho, N.J.; Kanazawa, K. Analyzing spur-distorted impedance spectra for the QCM. *Sensors* **2009**, *2009*, 259746. [[CrossRef](#)]
32. Lee, M.-H.; Park, S.-K.; Chung, C.-K.; Kim, H.-J. QCM study of  $\beta$ -casein adsorption on the hydrophobic surface: Effect of ionic strength and cations. *Bull. Korean Chem. Soc.* **2004**, *25*, 1031–1035.
33. Ozeki, T.; Verma, V.; Uppalapati, M.; Suzuki, Y.; Nakamura, M.; Catchmark, J.M.; Hancock, W.O. Surface-bound casein modulates the adsorption and activity of kinesin on SiO<sub>2</sub> surfaces. *Biophys. J.* **2009**, *96*, 3305–3318. [[CrossRef](#)]
34. Murray, B.S.; Cros, L. Adsorption of  $\beta$ -lactoglobulin and  $\beta$ -casein to metal surfaces and their removal by a non-ionic surfactant, as monitored via a quartz crystal microbalance. *Coll. Surf. B* **1998**, *10*, 227–241. [[CrossRef](#)]

35. Pérez-Fuentes, L.; Drummond, C.; Faraudo, J.; Bastos-González, D. Adsorption of milk proteins ( $\beta$ -casein and  $\beta$ -lactoglobulin) and BSA onto hydrophobic surfaces. *Materials* **2017**, *10*, 893. [[CrossRef](#)]
36. Reviakine, I.; Morozov, A.N.; Rossetti, F.F. Effects of finite crystal size in the quartz crystal microbalance with dissipation measurement system: Implications for data analysis. *J. Appl. Phys.* **2004**, *95*, 7712–7716. [[CrossRef](#)]
37. Nylander, T.; Tiberg, F.; Wahlgren, N.M. Evaluation of the structure of adsorbed layers of  $\beta$ -casein from ellipsometry and surface force measurements. *Int. Dairy J.* **1999**, *9*, 313–317. [[CrossRef](#)]
38. Fragneto, G.; Thomas, R.K.; Rennie, A.R.; Penfold, J. Neutron reflection study of bovine beta-casein adsorbed on OTS self-assembled monolayers. *Science* **1995**, *267*, 657–660. [[CrossRef](#)]
39. Tiberg, F.; Nylander, T.; Su, T.; Lu, J.; Thomas, R.  $\beta$ -casein adsorption at the silicon oxide–Aqueous solution interface. *Biomacromolecules* **2001**, *2*, 844–850. [[CrossRef](#)]
40. Jiang, X.; Wang, R.; Wang, Y.; Su, X.; Ying, Y.; Wang, J.; Li, Y. Evaluation of different micro/nanobeads used as amplifiers in QCM immunosensor for more sensitive detection of *E. coli* O157:H7. *Biosens. Bioelectr.* **2011**, *29*, 23–28. [[CrossRef](#)]
41. Dutta, A.K.; Nayak, A.; Belfort, G. Viscoelastic properties of adsorbed and cross-linked polypeptide and protein layers at a solid–liquid interface. *J. Coll. Interface Sci.* **2008**, *324*, 55–60. [[CrossRef](#)]
42. Tymchenko, N.; Nilebäck, E.; Voinova, M.V.; Gold, J.; Kasemo, B.; Svedhem, S. Reversible changes in cell morphology due to cytoskeletal rearrangements measured in real-time by QCM-D. *Biointerphases* **2012**, *7*, 43. [[CrossRef](#)] [[PubMed](#)]
43. Jian, J.-W.; Chiu, W.-C.; Chang, H.-T.; Hsu, P.-H.; Huang, C.-C. Fibrinolysis and thrombosis of fibrinogen-modified gold nanoparticles for detection of fibrinolytic-related proteins. *Anal. Chim. Acta* **2013**, *774*, 67–72. [[CrossRef](#)] [[PubMed](#)]
44. Chiu, W.-C.; Huang, C.-C. Combining fibrinogen-conjugated gold nanoparticles with a cellulose membrane for the mass spectrometry-based detection of fibrinolytic-related proteins. *Anal. Chem.* **2013**, *85*, 6922–6929. [[CrossRef](#)] [[PubMed](#)]
45. Chinnappan, R.; Al Attas, S.; Kaman, W.E.; Bikker, F.J.; Zourob, M. Development of magnetic nanoparticle based calorimetric assay for the detection of bovine mastitis in cow milk. *Anal. Biochem.* **2017**, *523*, 58–64. [[CrossRef](#)]
46. Weihs, F.; Peh, A.; Dacres, H. A red-shifted Bioluminescence resonance energy transfer (BRET) biosensing system for rapid measurement of plasmin activity in human plasma. *Anal. Chim. Acta* **2020**, *1102*, 99–108. [[CrossRef](#)]
47. Románszki, L.; Hianik, T.; Keresztes, Z. Plasmin determination based on enzymatic digestion of a  $\beta$ -casein layer at the air/water interface. *Coll. Surf. A* **2021**, *609*, 125786. [[CrossRef](#)]
48. Dizon, M.; Tatarko, M.; Szabo, K.; Hianik, T. Application of high-resolution ultrasonic spectroscopy for detection of the plasmin activity toward  $\beta$ -casein. *Food Chem.* **2021**, *353*, 129373. [[CrossRef](#)]
49. Tatarko, M.; Ivanov, I.N.; Hianik, T. New insights on plasmin long term stability and the mechanism of its activity inhibition analyzed by quartz crystal microbalance. *Micromachines* **2022**, *13*, 55. [[CrossRef](#)]
50. Leonil, J.; Molle, D.; Maubois, J.L. Study of the early stages of tryptic hydrolysis of  $\beta$ -casein. *Le Lait* **1988**, *68*, 281–294. [[CrossRef](#)]